



# Hysteretic energy-based state-dependent fragility for ground-motion sequences

Roberto Gentile<sup>1,2</sup> | Carmine Galasso<sup>1,3</sup>

<sup>1</sup> Department of Civil, Environmental and Geomatic Engineering, University College London, London, UK

<sup>2</sup> Institute for Risk and Disaster Reduction University College London, London, UK

<sup>3</sup> Scuola Universitaria Superiore (IUSS) Pavia, Pavia, Italy

## Correspondence

Roberto Gentile, Department of Civil, Environmental and Geomatic Engineering, University College London, London, United Kingdom.

Email: [r.gentile@ucl.ac.uk](mailto:r.gentile@ucl.ac.uk)

## Funding information

H2020 Marie Skłodowska-Curie Actions, Grant/Award Number: 843794

## Abstract

A framework to derive state-dependent fragility relationships of structures subjected to ground-motion sequences (e.g. mainshock-aftershock (MS-AS) or triggered earthquakes) is proposed. The hysteretic energy dissipated in the sequence is adopted as the main demand parameter, as it is a cumulative measure monotonically increasing with the length of the excitation. For a structure subjected to earthquake-induced ground motions, it is not possible to define a closed-form representation of the hysteretic energy as a function of the peak deformation. However, based on theoretical considerations, the hysteretic energy-peak deformation trend is discussed, highlighting that (a) the significant duration of the ground motion explains the variability of the hysteretic energy for a given peak deformation; (b) the hysteretic energy dissipated in an AS decreases (for a given AS peak displacement) if the peak displacement in the MS increases. A vector-valued probabilistic seismic demand model consistent with these considerations is proposed in the form of a surface relating the hysteretic energy in the sequence to the peak deformation in the MS and a ground-motion intensity measure of the AS. This is calibrated via sequential cloud-based time-history analyses. The framework is demonstrated for 14 reinforced concrete frame buildings with different height, plastic mechanisms, and infill distributions. The results show the feasibility of the proposed approach, effectively capturing damage accumulation without inconsistencies in the obtained statistical model. The framework may be used for risk-assessment applications explicitly incorporating ground-motion sequences. The hysteretic energy versus peak deformation relationship may also be exploited in problems involving long-duration ground motions or soft soils.

## KEYWORDS

ground-motion sequences, hysteretic energy versus peak deformation, mainshock-aftershock, probabilistic seismic demand model, reinforced concrete frames, seismic fragility

This is an open access article under the terms of the [Creative Commons Attribution](https://creativecommons.org/licenses/by/4.0/) License, which permits use, distribution and reproduction in any medium, provided the original work is properly cited.

© 2020 The Authors. *Earthquake Engineering & Structural Dynamics* published by John Wiley & Sons Ltd.

## 1 | INTRODUCTION AND MOTIVATION

In seismic design or performance assessment of structures, peak quantities (mainly displacements or drifts) are generally adopted to define both engineering demands and capacities at a global or member level. The seismic capacity of a structural system/member is usually defined in terms of deformation thresholds obtained through monotonic or, less frequently, cyclic experimental tests. There is a vast consensus on the effectiveness of such an approach for a large number of circumstances. However, disregarding cumulative engineering demand parameters, EDPs (e.g. hysteretic energy, cumulated ductility demand, number of cycles), may not provide an analyst with full control of the performance assessment process under certain circumstances in which low-cycle fatigue is relevant<sup>1,2</sup>. Examples of this condition are long-duration ground motions, ground motions on very soft soils, (multiple) ground-motion sequences. This paper specifically deals with ground-motion sequences in which a first ground motion (called mainshock, MS) is followed by a second one (called aftershock, AS, for simplicity), which can either be an actual AS or a ground motion related to a triggered event (with a different rupture zone with respect to the one responsible for the MS).

Some recent research attention has been devoted to the development of fragility relationships for MS-AS ground-motion sequences that explicitly depend on the damage state (DS) achieved by a structure in the MS (i.e. state-dependent fragility). Most studies derive seismic fragility in terms of maximum interstorey drift thresholds<sup>3-5</sup>, although in some cases this is considered in conjunction with the residual drift<sup>6</sup>. This may create inconsistencies in the resulting statistical models due to inappropriate consideration of damage accumulation. For instance, if the peak drift computed for an AS ground motion is smaller than the one due to the corresponding MS, the structure is conventionally allocated to a lower DS with respect to that of the MS, which is clearly an inconsistency. This can, in turn, result in fragility curve crossings between various DSs. This is mostly avoided (rather than solved) by (a) using appropriately scaled ground motion sequences, thus modifying the input signals; (b) disregarding the analysis cases for which the AS drift is smaller than the MS one, thus biasing the statistical result (for example, Zhang et al.<sup>6</sup>). As hysteretic energy is a cumulative measure that monotonically increases with the length of the applied excitation (see Changhai et al.,<sup>7</sup> for example), the above-mentioned inconsistency is automatically removed if hysteretic energy is used as an EDP. However, no probabilistic seismic demand model (PSDM) based on hysteretic energy has been proposed for MS-AS sequences to date.

Several studies explicitly included cumulative EDPs in the design/assessment process<sup>2,8-12</sup>. Arguably, it is challenging to estimate a member or global structural capacity in terms of cumulative EDPs, to define reliable DS thresholds, which are more easily (and widely) defined based on displacement/drift. However, there exists a stable, pseudoparabolic relationship between peak deformation and hysteretic energy. This was confirmed by numerical dynamic analyses of single degree of freedom (SDoF) systems subjected to ground motions<sup>13-15</sup> and quasi-static, cyclic experimental tests on single members<sup>16-19</sup>. It is worth stressing that the above statement refers to the cumulative definition of hysteretic energy for dynamic actions, calculated over the force-displacement time history (due to a given ground-motion record). The monotonic, quasi-static definition of the hysteretic energy is herein less relevant, as it could only serve as a phenomenological aid to distinguish systems with different hysteretic characteristics. In fact, these are two completely different quantities that are not correlated<sup>20-22</sup>. The work in this paper is based solely on the cumulative hysteretic energy.

Based on theoretical considerations on the peak deformation-hysteretic energy relationship, a PSDM is proposed here in the form of a surface relating the hysteretic energy in the MS-AS sequence to the peak deformation in the MS and a ground-motion intensity measure (IM) of the AS. The PSDM functional form, which embeds the peak deformation-hysteretic energy relationship itself, is defined consistently with the mechanics of a structure subjected to an MS-AS sequence. A procedure is finally proposed to derive state-dependent fragility relationships (i.e. representing the exceeding probability of a DS in the AS, conditioned on the IM of the AS, and the DS of the MS). The adopted EDP for the fragility relationships is the cumulative hysteretic energy in the MS-AS sequence. Therefore, the peak deformation-hysteretic energy relationship is used to convert the deformation-based DS thresholds into energy-based ones. This allows one to retain the reliability of the adopted DS thresholds, as the deformation-energy conversion can start from any widely accepted/validated, deformation-based EDP limit. It is proposed to calibrate the PSDM through a cloud-based nonlinear time-history analyses (NLTHA) using artificial MS-AS sequences assembled via a randomized approach<sup>5</sup>. This approach does not require a site-specific, hazard-consistent record selection (e.g. Papadopoulos et al.<sup>3</sup>), and requires none-to-moderate scaling of the ground motions. It is worth mentioning that catastrophic effects due to low-cycle fatigue (e.g. fracture of a rebar) are not explicitly considered herein as this effect is typically not explicitly included in the numerical models. As the proposed procedure is based on numerical analyses only, the results of this paper alone cannot fully confirm that hysteretic energy is an appropriate proxy for damage accumulation. However, together with relevant experimental/field data, the proposed procedure may be used to provide a deeper confirmation to such hypothesis.

This paper has the following specific objectives, addressed in the subsequent sections: (a) To qualitatively discuss the trend between hysteretic energy and peak deformation for individual ground-motion records or MS-AS sequences, identifying the parameters affecting such a trend based both on theoretical and empirical evidence; (b) to propose a PSDM for MS-AS conditions consistent with the relevant physics; (c) to derive state-dependent fragility models for realistic case studies. To this aim, a set of NLTHA is first carried out for a case-study SDoF system. Then, the proposed framework is demonstrated for 14 reinforced concrete (RC) frame buildings, characterized by different height levels (four or eight storeys), plastic mechanisms (beam sway, in which all the beams are yielding; column sway, with a soft-storey mechanism; mixed sway, in which a combination of beam, column, and/or joint failures can be triggered), configuration of the infill panels (bare frame, uniformly infilled frame, pilotis frame).

## 2 | PEAK DEFORMATION VERSUS HYSTERETIC ENERGY

For a structure subjected to a dynamic excitation, the energy dissipated through hysteresis is derived by adopting the energy balance equation. For an SDoF system, the force equilibrium (Equation 1) depends on the mass of the system  $m$ , the viscous damping coefficient  $c$ , the restoring force  $f_s$ , and the ground acceleration  $\ddot{u}_g$  ( $u$ ,  $\dot{u}$ ,  $\ddot{u}$  are the displacement, velocity, and acceleration relative to the ground, respectively). By multiplying such equation for the instantaneous displacement  $\dot{u}dt$ , and integrating over time, the energy balance equation (Equation 2) is obtained. The third term of this equation embeds, over time, the hysteretic energy and the stored elastic strain energy. However, if measured at the end of a ground-motion excitation, when the system has come to rest, the elastic strain energy is zero and the term refers to the hysteretic energy only.

$$m\ddot{u} + c\dot{u} + f_s(u, \dot{u}) = -m\ddot{u}_g \quad (1)$$

$$\int_t m\ddot{u}\dot{u}dt + \int_t c\dot{u}^2dt + \int_t f_s(u, \dot{u})\dot{u}dt = - \int_t m\ddot{u}_g\dot{u}dt. \quad (2)$$

A fundamental parameter affecting the hysteretic energy is  $f_s$ , which depends on the force-deformation backbone curve of the system and the set of hysteretic rules. The backbone curve describes the (tangent) stiffness of the system under monotonic, quasi-static loading, whereas the hysteresis describes how such stiffness evolves under cyclic conditions, that is, under unloading and reloading. More complete/advanced models also involve strength degradation, both within a single cycle or across multiple cycles. Within-cycle degradation depends on the maximum deformation (or ductility) demand and produces a modification of the backbone curve (usually corresponding to a negative slope). Cyclic degradation generally depends on the number of plastic excursions (i.e. when the response “leaves” the backbone curve). The combination of the above-mentioned parameters, together with the applied load history (e.g. a ground motion), determines the amount of hysteretic energy dissipated by a structure. The amount of viscous damping has a significant effect on the hysteretic energy (that is, the higher the damping, the lower the hysteretic energy).

For a realistic structure, damping depends on both material and lateral-load resisting system (e.g. steel frame vs. RC wall). Moreover, the modal properties of the structure affect hysteretic energy, especially if higher modes are relevant. Therefore, for a given material/lateral-load resisting system, this is indirectly controlled by the height of the structure. Most importantly, the plastic mechanism is a fundamental factor to consider, which is likely governed by the level of seismic design. This affects the members involved in the nonlinear dynamic response, and therefore both the monotonic and cyclic properties at global level.

Based on this discussion, any consideration about hysteretic energy cannot be generalized. For a given (archetype) structure, however, the ground-motion record is the most relevant parameter to consider when characterizing the energy versus deformation relationship. This is herein discussed first for single-record conditions, and then for MS-AS sequences, considering both an illustrative SDoF system and a realistic RC frame.

### 2.1 | Single ground-motion conditions

There exists a stable, pseudoparabolic relationship between the peak global displacement ( $\Delta_{max}$ ) and the hysteretic energy of a system,<sup>13–15</sup> herein called  $E_{H,MS}$  for consistency with the subsequent sections. To qualitatively confirm this trend, an illustrative SDoF system is analyzed via an incremental dynamic analysis, IDA<sup>23</sup>. The SDoF is defined by the backbone

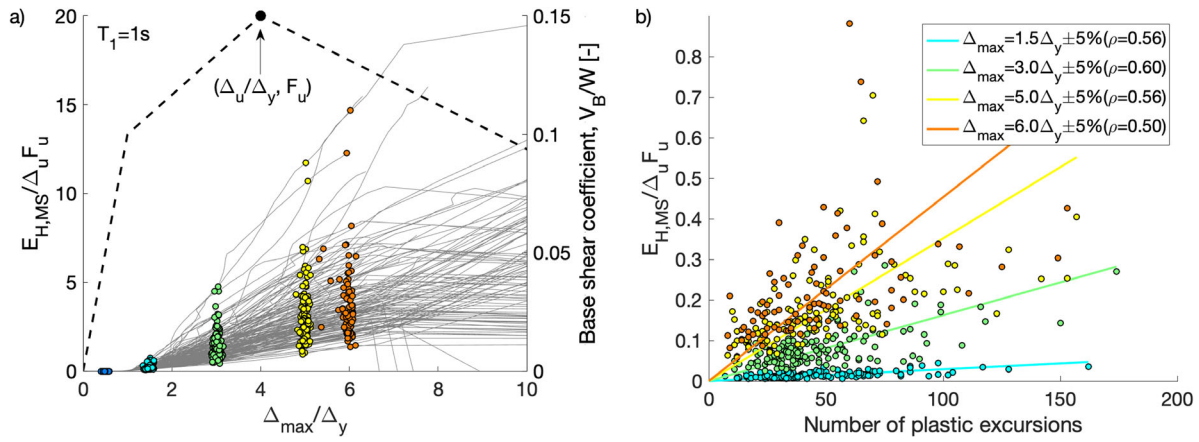


FIGURE 1 (a) Hysteretic energy versus maximum drift IDA curves for a case-study SDoF system (150 records); (b) hysteretic energy versus number of plastic excursions for different levels of displacement.  $T_1$ : fundamental vibration period;  $\rho$ : correlation coefficient

curve shown in Figure 1, assuming a modified Takeda hysteresis<sup>24</sup>, and a period of 1 s. No cyclic degradation is considered for simplicity. A single case study is deemed sufficient because according to previous studies<sup>22,25</sup>, for a given set of hysteretic rules, similar trends were encountered in the displacement versus energy behavior of SDoF systems having different periods, backbone curves, and hysteresis rules; however, the absolute values of the hysteretic energy are different depending on the above features. The IDA curves are represented in terms of hysteretic energy (normalized by the product of the peak force and related displacement,  $F_u \Delta_u$ ) versus peak displacement, which may be interpreted as a particularly efficient IM. The 150 records with highest peak ground acceleration (PGA) in the SIMBAD database<sup>26</sup> are arbitrarily used (the details of the record selection procedure can be found in Gentile et al.<sup>27</sup>). These records include a variety of conditions (geographical setting, fault styles, ordinary vs. pulse-like records, short vs. long-duration records, etc.).

Figure 1a shows a pseudo-bilinear trend for the energy-versus-displacement relationship for each record. This is because, for such a simple system, no hysteretic energy is dissipated for any peak displacement smaller than yielding. As shown later in the paper, such a trend becomes pseudoparabolic in the case of more complex systems (for which the transition between pre- and postyielding behavior is smoother). The pseudoparabolic trend may be well represented by the widely adopted power law model ( $E_{H,MS} = a\Delta_{max}^b$ ), as confirmed by various goodness-of-fit metrics. The scatter of ( $E_{H,MS}|\Delta$ ) is likely dependent on the number of plastic excursions registered in the response. Figure 1b shows scatter plots in terms of energy and plastic excursions for four different levels of peak displacement (above yielding). Regardless of the displacement level, the coefficient of correlation  $\rho$  falls in the range 0.56–0.60, therefore supporting the claim. As significant duration may be a good proxy for the number of plastic excursions, this parameter may be used to explain the variability of  $E_{H,MS}|\Delta$ . Indeed, the correlation coefficient between  $E_{H,MS}|\Delta$  and significant duration (5–95%) is within the range 0.6–0.7 for this example. This is in line with previous findings<sup>28</sup>, for which using the significant duration to form a compound IM, together with peak displacement, significantly improves the correlation with hysteretic energy. The median  $E_{H,MS}$  versus  $\Delta$  may be calibrated adopting a sufficiently large number of ground-motion records with a wide range of both peak intensity (e.g. spectral acceleration) and significant duration.

## 2.2 | Mainshock-aftershock sequence conditions

Given the higher complexity of MS-AS conditions with respect to the single-record condition discussed above, it is decided to first resort to a particularly simplified situation. An SDoF system with the same backbone as above is characterized by a kinematic hardening hysteresis (i.e. no stiffness degradation). This is subjected to a quasi-static load history composed by two half-cycle loadings (Figure 2a). The first half cycle (the MS) is represented by the path O-Y-MM-RM: it starts from zero, reaches the displacement  $\Delta_{max}^{MS}$ , passing through the yielding point, and ends at the residual displacement  $\Delta_{res}^{MS}$  (defined only by  $\Delta_{max}^{MS}$  and the initial stiffness). The second half cycle (the AS) is defined by the path RM-MM-MA-RA: it starts from the residual displacement in the MS  $\Delta_{res}^{MS}$ , reaches the maximum displacement in the AS ( $\Delta_{max}^{AS}$ ) (passing through the evolved yielding point,  $\Delta_{max}^{AS}$ ), and ends at a residual displacement for the AS ( $\Delta_{res}^{AS}$ ).

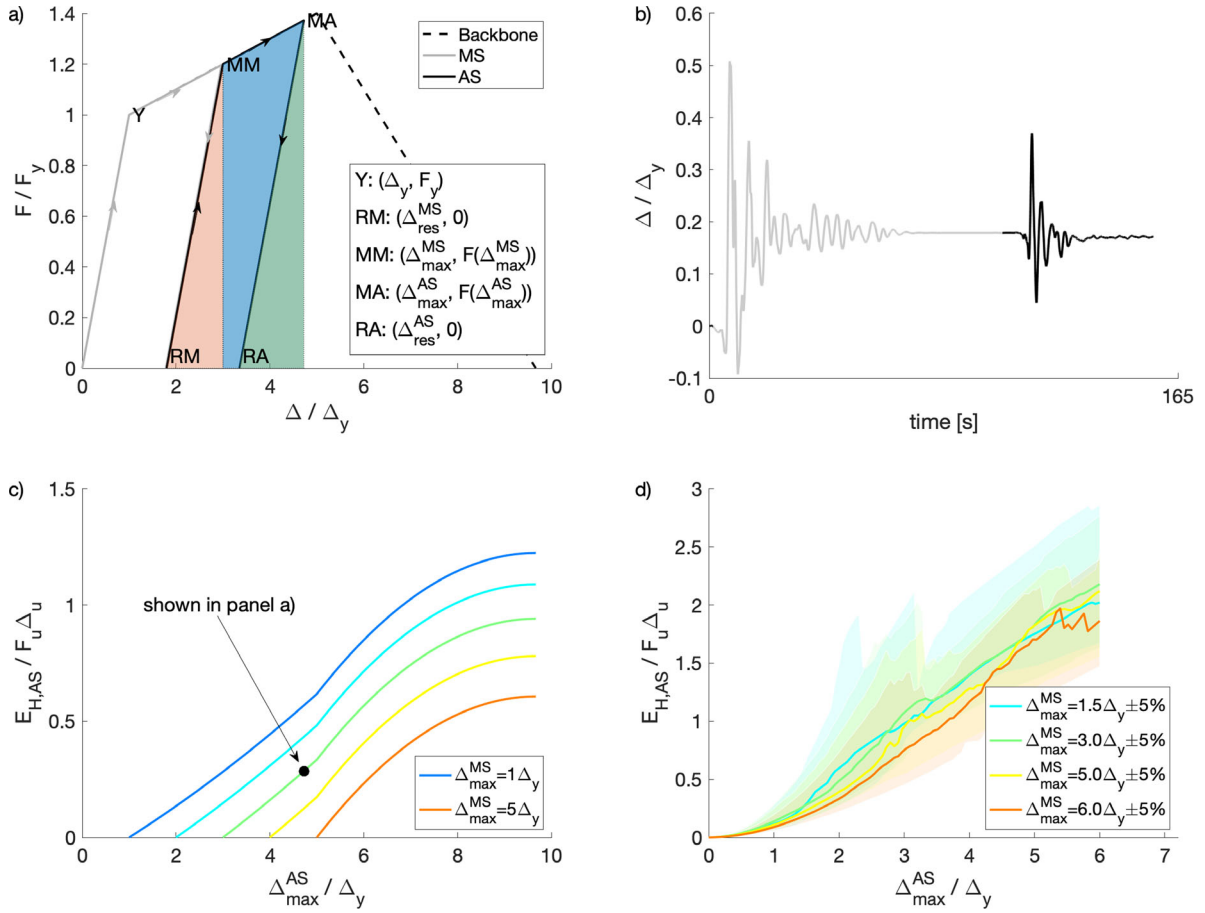


**FIGURE 2** Case-study SDoF system. (a) Load path for a quasi-static condition; (b) Displacement response for one realistic ground-motion sequence; (c) Aftershock hysteretic energy versus maximum drift relationship for the quasi-static condition; (d) Aftershock hysteretic energy versus maximum drift relationship for the ground-motion sequences loading (double IDA with  $10 \times 10$  records)

Such a simple load condition is chosen because it allows one to analytically evaluate the hysteretic energy. Although simplified, such a theoretical case helps the discussion of more complex conditions (e.g. SDoF systems or realistic structures subjected to MS-AS sequences). The expression for the hysteretic energy in the AS,  $E_{H,AS}$  (for an  $\Delta_{max}^{AS}$  not reaching the degrading branch), is shown in Equation 3, in which  $F$  is the base shear. The shaded areas in Figure 2a represent the three terms of the second member in Equation 3, which, respectively, correspond to the trapezoid  $MM'-MM-MA-MA'$ , and the triangles  $RM-MM-MM'$  and  $RA-MA-MA'$  ( $MM'$  and  $MA'$  are the projections on the horizontal axis of the points  $MM$  and  $MA$ ). Extending the calculation for load histories with the point  $MA$  in the degrading branch is trivial and it is not shown for brevity. Clearly, by setting  $\Delta_{max}^{MS} = \Delta_{res}^{MS} = 0$ , the calculated hysteretic energy refers to the MS.

$$E_{H,AS} = \frac{(F(\Delta_{max}^{AS}) + F(\Delta_{max}^{MS}))(\Delta_{max}^{AS} - \Delta_{res}^{MS})}{2} + \frac{(\Delta_{max}^{MS} - \Delta_{res}^{MS})F(\Delta_{max}^{MS})}{2} - \frac{(\Delta_{max}^{AS} - \Delta_{res}^{MS})F(\Delta_{max}^{AS})}{2}. \quad (3)$$

Figure 2c shows this equation for different values of  $\Delta_{max}^{MS}$ . For a peak displacement  $\Delta_{max}^{AS}$  smaller or equal to the start of the degrading branch, the  $E_{H,AS}(\Delta_{max}^{AS})$  relationship is parabolic with a fairly small concavity (confirming past findings, e.g. Bojórquez et al.<sup>29</sup>). For larger displacements (i.e. the point  $MA$  falls in the degrading branch of the backbone), where the tangent stiffness is negative, the  $E_{H,AS}(\Delta_{max}^{AS})$  relationship changes concavity and reaches a maximum for a displacement corresponding to a zero force in the backbone. Most importantly, for a given value of  $\Delta_{max}^{AS}$ , there is a decreasing, linear relationship between  $E_{H,AS}$  and  $\Delta_{max}^{MS}$ , as the different curves in Figure 2c are equally spaced. Therefore, the SDoF system dissipates less energy (for a given  $\Delta_{max}^{AS}$ ), if the dissipation in the MS is higher (which is proportional to  $\Delta_{max}^{MS}$ ).

To confirm the above considerations for more complex conditions, the above-mentioned SDoF system (with Takeda hysteresis) is analyzed via a double IDA approach. First, 10 records are randomly selected among the ones presented

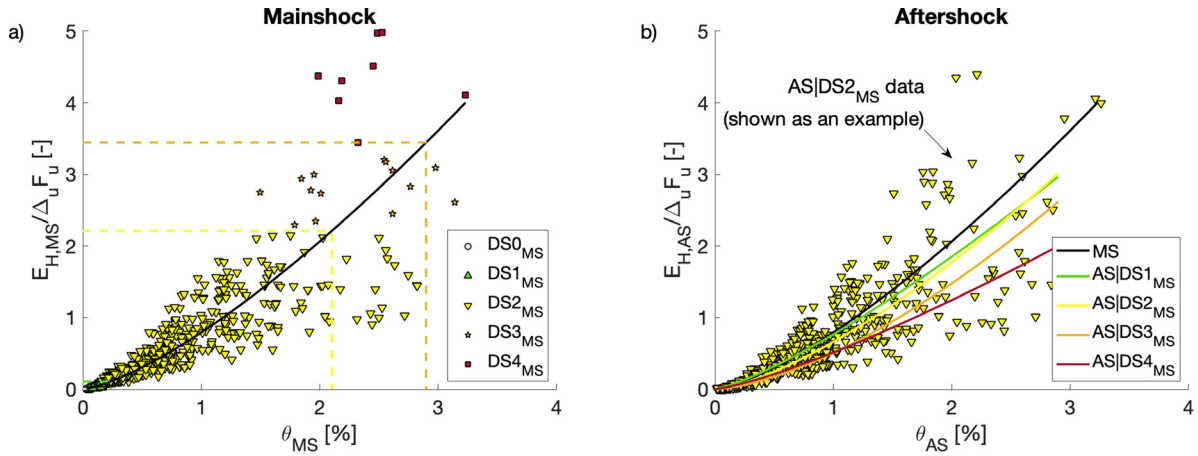


FIGURE 3 Hysteretic energy versus maximum interstorey drift relationship for a case-study RC frame. (a) Mainshock; (b) aftershock (dependent on the damage state in the mainshock)

in Figure 1a, considering the scale factors that cause four different levels of  $\Delta_{max}^{MS}$  (greater than yielding). Each of these (scaled) records is considered as the MS, and the double IDA is performed assembling each of them with the 10 records in the suite, which are increasingly scaled. Forty seconds free vibration time is allowed between the MS and the AS, such that the system can reach the rest configuration. Figure 2c shows the displacement response of the SDoF for one randomly chosen ground-motion sequence in the double IDA. For each level of “conditioning”  $\Delta_{max}^{MS}$ ,  $10 \times 10$  IDA curves are available. Figure 2d shows the median and 5–95% confidence bounds of the IDA curves, represented in terms of  $E_{H,AS}$  versus  $\Delta_{max}^{AS}$ . It is worth mentioning that  $\Delta_{max}^{AS}$  is calculated relatively to  $\Delta_{res}^{MS}$ . The results confirm the above discussion, particularly considering that the higher is the dissipated energy in the MS (proportional to  $\Delta_{max}^{MS}$ ), the lower is the dissipated energy in the AS (for a given  $\Delta_{max}^{AS}$ ). This may not seem to apply for  $\Delta_{max}^{AS}/\Delta_y$  in the range [4.5–6], where for the median  $E_{H,AS}$  relationship related to  $\Delta_{max}^{MS}$  equal to  $3\Delta_y$  or  $5\Delta_y$  is above the one related to  $1.5\Delta_y$ . This is related to the low number of sequences used for this example: in Figure 2c, only 10 ground-motion sequences are adopted for each  $\Delta_{max}^{MS}$  level. It is finally worth mentioning that such an inconsistency completely disappears if hundreds (rather than tens) of ground-motion sequences are used (as shown in Figure 3b).

To further generalize the discussion, a realistic RC frame is also considered. The details of the case study (i.e. Beam-Sway, four-storey frame below) are deemed less relevant here. However, a full description of the geometry, material properties, and structural details is given in Section 4.1 while the nonlinear modeling strategy for the time-history analyses is given in Section 4.2. The frame is analyzed via a cloud-based approach using MS-AS sequences obtained randomly assembling natural ground-motion records. The details of this approach, also describing the 1000 considered sequences, are given in Section 3.1. Figure 3a shows the results of the analyses in terms of hysteretic energy versus maximum interstorey drift for MSs only. The proposed law  $E_{H,MS} = a\theta_{MS}^b$  is fitted to the obtained data. This curve is used to define energy-based DS thresholds starting from drift-based ones (as discussed in detail in Section 4.1). The  $E_{H,AS}$  versus  $\theta_{AS}$  data are partitioned based on the DS achieved in the MS, and further power-law models are fitted to each subset of data. They are shown in Figure 3b, in which only the points related to DS2 in the MS are shown to improve the clarity of the plot. It is worth mentioning that the AS drift is calculated relative to the residual MS drift. The results clearly confirm the above discussion: for a given value of  $\theta_{AS}$ , the  $E_{H,AS}$  values are lower for a higher DS in the MS (corresponding to a higher  $E_{H,MS}$  and  $\theta_{MS}$ ). It is worth repeating that the absolute value of the fitting parameters ( $a$ ,  $b$ ) are strongly dependent on the backbone, hysteresis, and degradation properties of the considered structure, in turn dependent on the material, lateral-load resisting system, dynamic properties, etc.

### 3 | PROPOSED PROCEDURE TO DERIVE STATE-DEPENDENT FRAGILITY RELATIONSHIPS

The proposed procedure for state-dependent fragility analysis is based on a cloud-based approach<sup>30</sup> to NLTHAs using ground-motion sequences composed of two real (i.e. recorded) ground motions (herein called MS and AS, for simplicity).

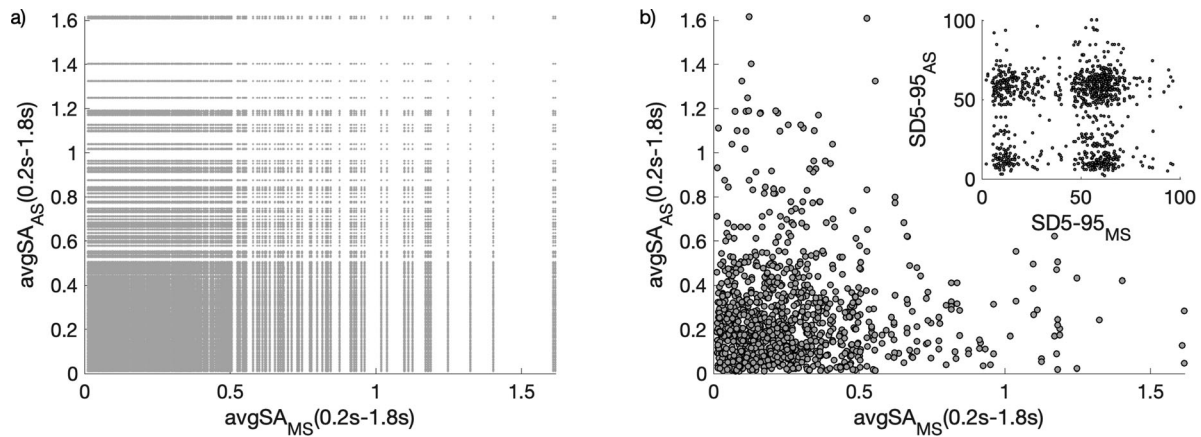


**FIGURE 4** Scatter of  $avgSA$  for mainshock (MS) versus aftershock (AS). (a) All possible pairs (391,876 sequences); (b) randomly selected 1000 sequences via the Latin hypercube sampling approach. SD5-95:

For each considered sequence, the maximum interstorey drift and the hysteretic energy are registered in both the MS and AS. Such data are used to calibrate a five-parameter PSDM represented by a surface depending on the maximum response in the MS and the IM of the AS.

For any set of drift-based DS thresholds (selected by the user), the above PSDM is used to derive the corresponding thresholds based on the (normalized) hysteretic energy. It is assumed that the energy-based thresholds remain unchanged regardless of the demand in the AS. Although it is fundamental to validate this assumption (which may be affected, for instance, by catastrophic failures due to low-cycle fatigue), this is considered out of scope herein, given the numerical nature of this study.

A set of lognormal fragility relationships is fitted: for the undamaged structure (using the hysteretic energy in the MS as an EDP) and for each considered DS in the MS (using the sum of the MS-AS hysteretic energy). It is worth noting that the lognormal distribution was demonstrated as appropriate for fragility relationships in terms of hysteretic energy.<sup>29</sup>

### 3.1 | Assembled ground-motion sequences

Past studies adopted real (i.e. as recorded) MS-AS sequences (e.g. Zhang et al.<sup>6</sup>). However, due to the low availability of sequences with strong ASs, this often limits the observations of significant damage increase due to sequential excitations. In turn, this does not allow developing statistically robust fragility models conditioned on the initial DS due to the MS. To overcome this, while avoiding the use of synthetic ground motions<sup>31</sup> or substantial amplitude scaling of real records (e.g. IDA), a randomized approach based on real records is adopted, as done in Aljawhari et al.<sup>5</sup> The resulting artificial sequences may represent multiple ground shaking that may occur in the form of typical ASs or triggered events. The seed ground motions (crustal only) are collected from three different databases: (a) the 2012 KKiKSK ground-motion database;<sup>32</sup> (b) the database developed by Goda and Taylor;<sup>33</sup> (c) the 100 records with the highest PGA in the SIMBAD Database.<sup>26</sup> The relevant seismological parameters (e.g. magnitude and source-to-site distance ranges, soil types) are reported in Aljawhari et al.<sup>5</sup> By separately considering both horizontal components of such records (MS only), 626 ground motions are selected. It is worth mentioning that this arbitrary selection of records is consistent with the adopted cloud-based response analysis approach, which does not require a hazard-consistent suite of ground-motion records.

By combining two records (herein called MS and AS, for convenience), artificial sequences are assembled, also allowing 40 s of free vibration in between. Instead of considering all the possible combinations (391,876; shown in Figure 4a), 1000 random pairs are selected adopting the Latin hypercube sampling approach. The interval [0,626], where 626 is the total number of seed ground motions, is subdivided in 1000 equal-length bins, randomly extracting one sample from each bin (based on a uniform distribution). Rounding up the result provides integer values corresponding to the actual ground-motion index in the database. This process is repeated twice, and the results are randomly combined, without repetition, to generate 1000 pairs of integers defining the assembled sequences. Figure 4b illustrates the values of the geometric mean of the 5%-damped pseudo-spectral acceleration in a range of periods ( $AvgSA$ ) for the MS and AS in each sequence. This ensures increased efficiency and (relative) sufficiency in estimating a given EDP by means of a scalar IM, as it is

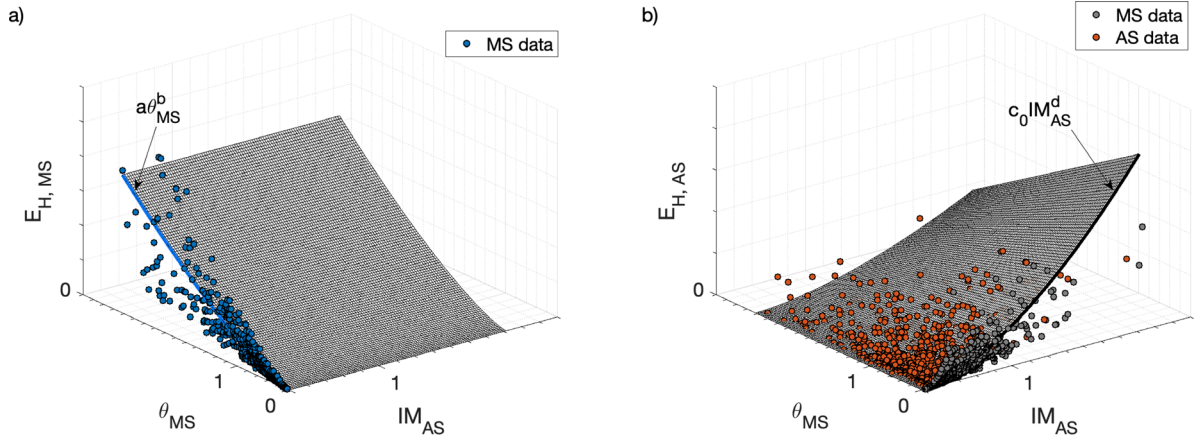


FIGURE 5 Derivation of the probabilistic seismic demand model. (a) Mainshock; (b) aftershock

able to account for higher mode effects and period elongation.<sup>34</sup> The range of periods [0.2–1.8 s] is herein selected for illustration purposes only. It is clear that this randomized selection method allows reducing the computational burden for the NLTHAs, while keeping a wide variety of low and high IM levels for both MS and AS.

### 3.2 | Probabilistic seismic demand model

The proposed PSDM is the surface  $E_{H,MSAS}(\theta_{MS}, IM_{AS})$ , where  $\theta_{MS}$  is the maximum interstorey drift in the MS and  $IM_{AS}$  is an IM in the AS (e.g. *AvgSA*). A fundamental requirement for any PSDM is the consistency with the physics of the problem under investigation. Based on the discussion in Section 2, consistency with the relevant mechanics is achieved if (a) the median hysteretic energy dissipated during the sequence is monotonic with respect to (any combination of) the maximum response in the MS and the IM of the AS. In other words, the gradient of  $E_{H,MSAS}(\theta_{MS}, IM_{AS})$  must be positive regardless of both the position and direction in the plane  $(\theta_{MS}, IM_{AS})$ , for physically sound ranges of both  $\theta_{MS}$  and  $IM_{AS}$ ; (b) for any given value of  $IM_{AS}$ ,  $E_{H,AS}$  must be monotonically decreasing with respect to  $\theta_{MS}$ . As an additional (not strictly necessary) condition, the proposed PSDM is required to be consistent with the power-law relationship commonly adopted for cloud-based MS-only problems (it must be its generalization). In other words, predicting the MS response with the proposed PSDM must give the same result as the power-law model.

The functional form of the PSDM is given in Equations 4 and 5, in which the MS and AS hysteretic energy values are treated separately and then summed. The model depends on five parameters ( $a$ ,  $b$ ,  $c_0$ ,  $d$ , and  $m$ ), which are estimated through regression.

$$E_{H,MSAS} = E_{H,MS} + E_{H,AS} = a\theta_{MS}^b + c(\theta_{MS})IM_{AS}^d \quad (4)$$

$$c(\theta_{MS}) = (1 - m\theta_{MS})c_0. \quad (5)$$

Figure 5a shows the MS portion of the hysteretic energy, together with an example scatter of the MS data. Clearly, such data lie in the  $(\theta_{MS}, E_{H,MS})$  plane and, according to the discussion in Section 2, it may be fitted with the power law relationship  $a\theta_{MS}^b$ . Such relationship is monotonically increasing as a function of  $\theta_{MS}$  and clearly constant as a function of  $IM_{AS}$ . Figure 5b, on the other hand, shows the AS portion of the hysteretic energy together with the AS scatter data  $(\theta_{MS}, IM_{AS}, E_{H,AS})$ . In the  $(IM_{AS}, E_{H,AS})$  plane, the MS data are also shown (therefore for  $\theta_{MS} = 0$ ). This is possible considering that an MS can be interpreted as an AS that follows an MS producing zero drift (i.e. an AS that follows no MS is a MS itself). This consideration allows calibrating the relationship  $E_{H,MSAS}(\theta_{MS} = 0) = c_0 IM_{AS}^d$  using the MS data only. In this way, using this PSDM for MS-only predictions will provide, by definition, the same result as the simple power-law model. Finally, the factor  $c(\theta_{MS}) = (1 - m\theta_{MS})c_0$  allows to linearly reduce the “slope” of the  $c_0 IM_{AS}^d$  relationship as a function of  $\theta_{MS}$ , consistently with the discussion in Section 2.2, and with requirement (b). This function is fitted

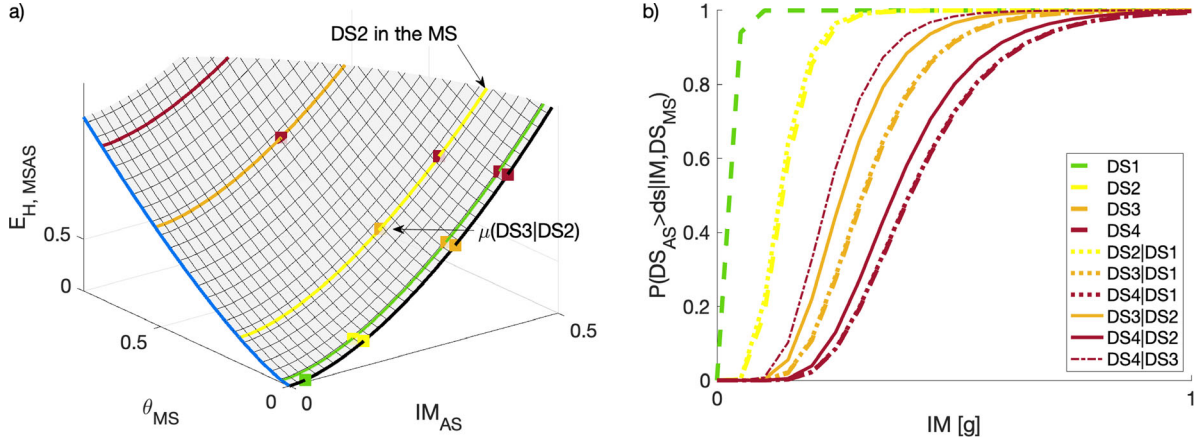


**FIGURE 6** (a) Probabilistic seismic demand model; (b) state-dependent fragility functions. *Note:* In panel b, the line type represents the conditioning damage state ( $DS_{MS}$ ) while the line color represents the achieved damage state ( $DS_{AS}$ ). For example, the red dotted line represents  $DS_{MS} = 1$  and  $DS_{AS} = 4$

using the AS data ( $\theta_{MS}$ ,  $IM_{AS}$ ,  $E_{H,AS}$ ). Based on these considerations,  $E_{H,MSAS}$  has indeed a positive gradient for physically sound ranges of both  $\theta_{MS}$  and  $IM_{AS}$  (satisfying requirement (a) above). It is worth mentioning that the dynamic analyses leading to “collapse” are herein disregarded and the information carried out by such data can be considered when deriving the fragility relationships. This can be done by characterizing the probability of collapse with a logistic model, as described in Section 3.3. Collapse herein corresponds to a global dynamic instability of the numerical analysis (i.e. nonconvergence), likely corresponding to a plastic mechanism (i.e. the structure is underdetermined) or exceeding a conventional 10% maximum interstorey drift.

The steps to fit the proposed PSDM are herein summarized:

1. Using the MS data only ( $\theta_{MS}$ ,  $E_{H,MS}$ ), the relationship  $a\theta_{MS}^b$  is fitted. The parameters  $a$  and  $b$  are estimated via the linear least squares method in the log-log space
2. Using the MS data only ( $IM_{MS}$ ,  $E_{H,MS}$ ), the relationship  $c_0IM_{AS}^d$  is fitted. The parameters  $c_0$  and  $d$  are estimated as per point 1.
3. Using the AS data ( $\theta_{MS}$ ,  $IM_{AS}$ ,  $E_{H,AS}$ ), the parameter  $m$  is estimated via the nonlinear least squares to the function  $E_{H,AS} = (1 - m\theta_{MS}) c_0IM_{AS}^d$ .

### 3.3 | State-dependent fragility analysis

The proposed PSDM is used to derive state-dependent fragility relationships in the form of lognormal cumulative distribution functions. As shown in Figure 6a (mixed-sway four-storey case study, below), after selecting the drift thresholds ( $\overline{\theta}_{DS}$ ) for an arbitrary number  $N$  of DSs, the PSDM will automatically provide their conversion in terms of hysteretic energy thresholds ( $\overline{E}_{H,DS}$ ). Equation 6 allows deriving fragility relationships for different combinations of the DS in both the MS and AS, specified as  $F(DS_{AS}|DS_{MS})$ . In such equation, the cumulative MS-AS hysteretic energy (previously referred to as  $E_{H,MSAS}$ ) is referred as  $E_H$ , for brevity. Practically,  $F(ds|0)$  are the MS fragilities (with  $ds = 1 \dots N$ ), while  $F(DS_{AS}|DS_S)$  represent the AS fragility conditioned on a given DS in the MS. In the latter condition,  $DS_{AS} = DS_{MS} + 1, \dots, N$ , that is they represent the exceeding probability of the AS causing a “jump” to a higher DS with respect to the MS, conditioned to  $IM_{AS}$ . In such equation,  $\mu_{\ln E_H|DS_{MS}, IM_{AS}}$  is the fragility median (also called  $\mu(DS_{AS}|DS_{MS})$ , for simplicity) while  $\sigma_{\ln E_H|DS_{MS}, IM_{AS}}$  is the logarithmic standard deviation of the proposed PSDM.

$$F(DS_{AS}|DS_{MS}) = P\left(E_H \geq \overline{E}_{H,DS_{AS}} | DS_{MS}, IM_{AS}\right) = 1 - \Phi\left(\frac{\ln \overline{E}_{H,DS_{AS}} - \mu_{\ln E_H|DS_{MS}, IM_{AS}}}{\sigma_{\ln E_H|DS_{MS}, IM_{AS}}}\right). \quad (6)$$

Using the drift threshold for  $DS_{MS}$  and the energy threshold for  $DS_{AS}$ , and inverting Equation 4, the median of a given fragility curve is calculated (Equation 7). Equation 8 provides the dispersion of the fragility relationships, starting from

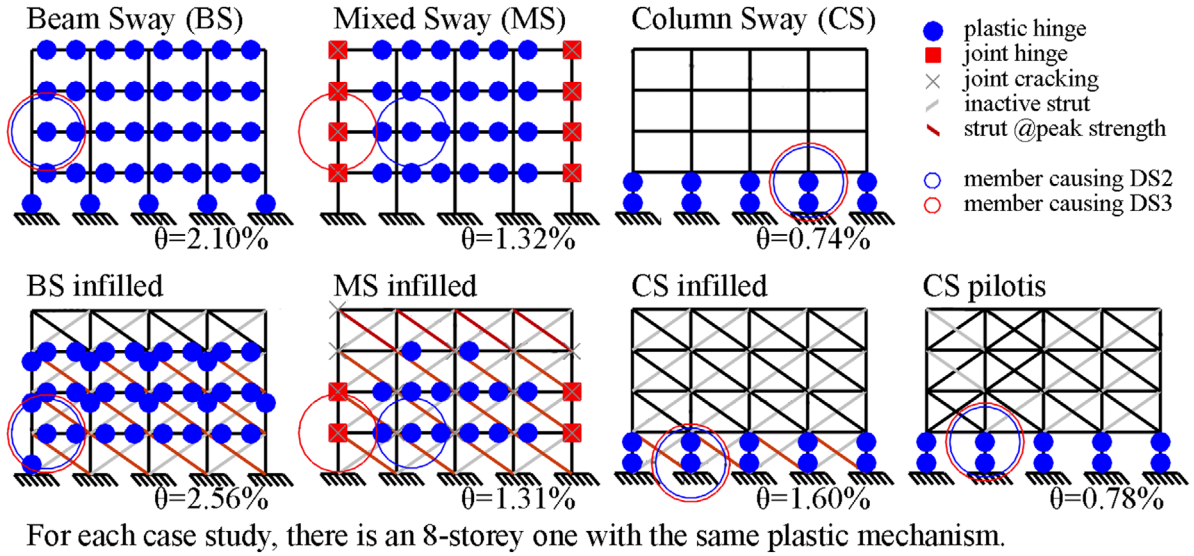


FIGURE 7 Plastic mechanism (DS3) for the analyzed case studies (eight-storey ones are not shown for brevity).  $\theta$ : maximum interstorey drift

the logarithmic standard deviation (from the PSDM). The resulting fragility relationships are shown in Figure 6b. As a direct consequence of having a monotonically increasing PSDM (see Section 3.2), the median of the AS fragility curves, for a given  $DS_{AS}$ , decreases as  $DS_{MS}$  increases. This means that damage accumulation is captured in a consistent and physically sound fashion.

It is worth repeating that the information carried out by the “collapse” analysis cases (dynamic instability or exceeding 10% drift), initially not considered in fitting the PSDM, can be accounted for here. Although this is not done here for simplicity, the probability of collapse can be represented by a generalized regression model with a “logit” link function (logistic regression), which is appropriate for cases in which the response variable is binary (in this case, “collapse” or “no collapse”). Then, the total probability theorem can be used to modify any of the calculated fragility curves, as shown in Jalayer et al.<sup>30</sup>

$$\mu_{\ln E_H | DS_{MS}, IM_{AS}} = \mu(DS_{AS} | DS_{MS}) = \left( \frac{E_{H, DS_{AS}} - a \theta_{DS_{MS}}^b}{c_0 (1 - m \theta_{DS_{MS}})} \right)^{1/d} \quad (7)$$

$$\beta = \sigma_{\ln E_H | DS_{MS}, IM_{AS}} / d. \quad (8)$$

## 4 | ILLUSTRATIVE APPLICATIONS

### 4.1 | Selected case studies

The proposed framework for state-dependent fragility analysis is demonstrated for 14 RC frames case studies (Figure 7). They have four bays and either four or eight storeys (the storey weight is approximately equal to 2017 kN). For each geometrical configuration, three different solutions are adopted for the seismic design and detailing of the RC members, leading to three different expected plastic mechanisms: beam sway (all beams and the base columns yield), mixed sway (combination of joint shear failures with beam and/or column flexure, shear, or lap-splice failures), and column sway (soft storey mechanism at ground storey). The beam-sway case studies are designed according to direct displacement-based design<sup>35</sup> assuming a medium seismicity (PGA = 0.25 g) according to the New Zealand load standard.<sup>36</sup> Capacity design principles are ensured for these frames, also including the minimum requirements for structural details according to the New Zealand design standards.<sup>37</sup> The mixed-sway frames have similar strength with respect to the beam-sway ones,

TABLE 1 Drift-based DS thresholds [%]

	Four storeys							Eight storeys						
	Bare			Uniformly infilled			Pilotis	Bare			Uniformly infilled			Pilotis
	BS	MS	CS	BS	MS	CS	CS	BS	MS	CS	BS	MS	CS	CS
$T_1$ [s]	0.48	0.50	1.06	0.18	0.19	0.22	0.99	0.97	1.02	1.19	0.38	0.38	0.44	0.82
DS1	0.03	0.03	0.08	0.03	0.03	0.05	0.08	0.14	0.17	0.05	0.02	0.01	0.04	0.06
DS2	0.24	0.19	0.42	0.19	0.19	0.18	0.44	0.34	0.33	0.27	0.18	0.17	0.17	0.31
DS3	2.10	1.32	0.74	2.56	1.31	0.60	0.78	2.91	1.37	0.66	3.17	1.36	0.69	0.73
DS4	2.90	1.76	0.99	3.16	1.74	0.83	1.05	3.92	1.82	0.95	4.39	2.21	1.08	0.99

Abbreviations: BS, beam sway; MS, mixed sway; CS, column sway;  $T_1$ , fundamental period

but they do not meet any minimum requirement for the structural details. This leads to a similar peak base shear in the pushover curve, but a considerably lower ductility capacity. The column-sway frames are designed for gravity loads only. The reader is referred to Gentile et al.<sup>38</sup> for details on the design of the case studies, the member detailing of each RC member, the adopted material models, the load analysis, and mass properties.

For each plastic mechanism configuration, both a bare and a uniformly infilled configuration are considered. Finally, a pilotis configuration (infills missing at the ground floor) is also considered for the column-sway cases. Such case studies could be also considered as “archetype” structures representative of different vulnerability classes in various earthquake-prone regions of the world. Four structure-specific DSs are assumed to derive fragility curves: slight, moderate, extensive, and complete damage (DS1–DS4). Those DSs are qualitatively defined according to HAZUS, HAZard United States,<sup>39</sup> and quantified for each case study using the pushover analyses results for each analyzed model. The plastic mechanisms of the four-storey frames, measured at the onset of DS3, are shown in Figure 7. Other definitions of the DSs are possible and the proposed framework is independent of their particular choice. The drift-based DS thresholds are shown in Table 1. As mentioned above, the corresponding thresholds based on hysteretic energy are derived using the fitted PSDMs.

## 4.2 | Numerical modeling strategy

NLTHA are carried out for refined 2D numerical models defined using the finite-element software Ruaumoko.<sup>40</sup> A tangent stiffness-proportional damping equal to 5% of the critical one is adopted for all the vibration modes. P-Delta effects are considered in the analyses. The modeling strategy is based on an experimentally validated<sup>41</sup> lumped plasticity approach. Mono-dimensional Giberson elements<sup>42</sup> are adopted for beams and columns. The end sections of the beams are characterized by a trilinear moment-curvature relationship, and equivalent plastic hinge length.<sup>35</sup> Axial load-moment interaction diagram and plastic hinge length are used for columns. The software RCsection<sup>43</sup> is used for the moment-curvature analyses and the potential flange effect is accounted for with a 30% increase in the negative moment capacity of the beams. Other failure mechanisms (i.e. flexure, bar buckling, lap-splice failure, shear) are evaluated, considering that the weakest link will govern the member ultimate strength and deformation. The modified Takeda hysteresis<sup>24</sup> is adopted for beams and columns. For the beams, the unloading and reloading stiffness factors are, respectively, equal to 0.3 and 0.5, while the columns have a thinner loop (the factors are, respectively, equal to 0.5 and 0).

To model the joint panels, the rigid ends of the adjacent beams and columns are connected with nonlinear lumped springs (two for each geometrical node of the frame). The nonlinear behavior of these springs is set consistently with the equivalent column moment-joint drift relationships.<sup>44</sup> Beam-column joints are consistent with the Modified Sina model,<sup>24</sup> which allows to consider a pinching behavior. The unloading/reloading stiffness factors are equal to 0.5 and 0, while pinching moment (corresponding to zero deformation) is equal to 25% of the strength. Within-cycle strength degradation of beams, columns and joint panels are set such that a negative stiffness branch in their backbone curves starts from their ultimate capacity and ends (with zero residual strength) at twice the ultimate capacity. The cyclic degradation is set such that strength reduces by 5% at the first plastic excursion. Such reduction exponentially decreases as the number of plastic excursions increases.

Infill panels are modeled using a modified version of the typical single equivalent strut approach. In such refinement, the pinned ends of each strut are connected to the beam and column interfaces with the joint panels by means of two rigid arms (one horizontal, one vertical) able to sustain axial load only. This allows to transfer the vertical and horizontal com-

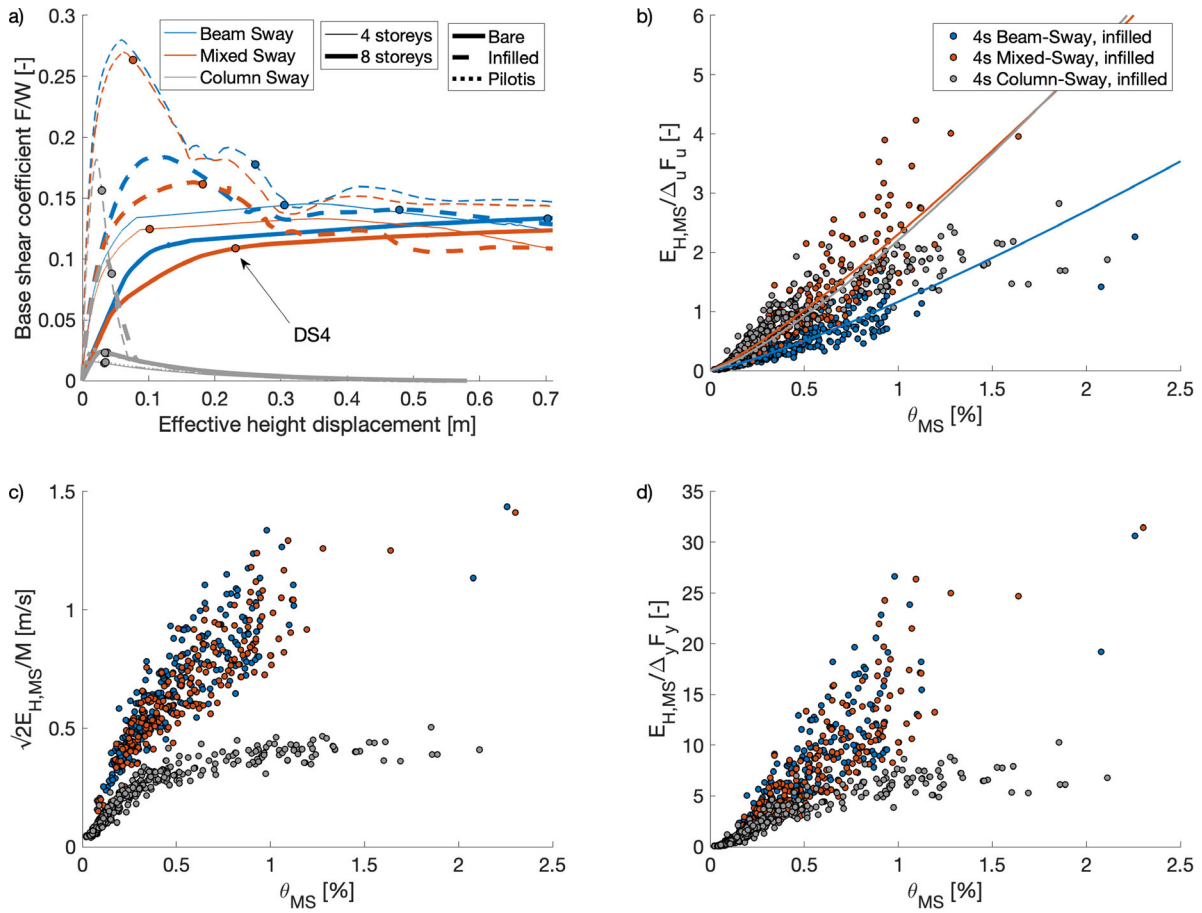


**FIGURE 8** (a) Normalized pushover curves.  $F$ : base shear,  $W$ : total weight; (b) normalized hysteretic energy versus maximum interstorey drift for the four-storey infilled case studies.  $\Delta_y, F_y$ : displacement and base shear at yielding (DS2);  $\Delta_u, F_u$ : displacement and base shear at damage state 4;  $M$ : total mass

ponent of the axial load of the strut by means of shear demand for the beam and the column, respectively. The Crisafulli hysteresis is adopted,<sup>45</sup> which embeds the within-cycle strength degradation. No cyclic degradation is considered for the infills.

Fully fixed boundary conditions are considered at the base, and floor diaphragms are modeled as rigid in plane. The numerical modeling is validated using pushover analyses (in displacement control and linear force profile) that are compared with analytical calculations through the simple lateral mechanism analysis (SLaMA).<sup>38,44,46,47</sup>

### 4.3 | Discussion

Figure 8a shows the pushover curves for all the considered case studies. Those are represented in terms of displacement at the effective height<sup>35</sup> and base shear normalized with respect to the total weight. The effective height displacement is obtained interpolating the displacement profile ( $\Delta_i$ ) of any analysis step at the effective height  $H_e = \sum m_i \Delta_i H_i / \sum m_i \Delta_i$ , where  $m_i$  and  $H_i$  are the mass and the height from the ground of storey  $i$ , respectively. It is clear how the four-storey frames are consistently stronger than the corresponding eight-storey ones, while having a higher DS4 displacement. The mixed-sway frames have a slightly smaller strength with respect to the corresponding beam-sway ones, while having a substantially lower displacement at DS4. The column-sway case studies show a particularly low strength and deformation capacity, together with a remarked degrading behavior. For the beam- and mixed-sway frames, the degrading behavior starts at particularly large displacements. As expected, the presence of the infills causes both a strength and stiffness increase for small displacements, followed by a sudden drop due to their pronounced degrading behavior. The pilotis column-sway frames show practically the same behavior as the column-sway bare ones.

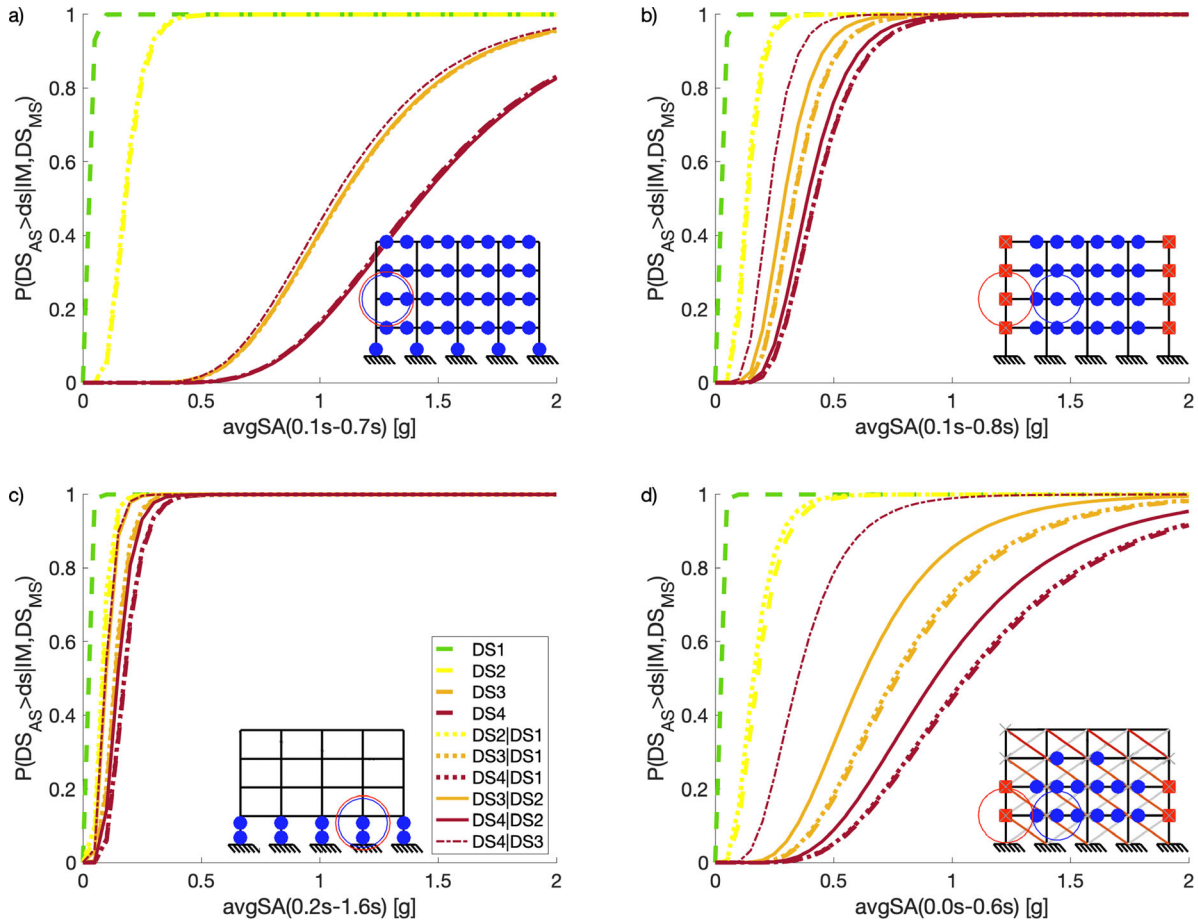


**FIGURE 9** State-dependent fragility (four-storey frames). (a) Beam sway; (b) mixed sway; (c) column sway; (d) mixed sway infilled. *Note:* The line type represents the conditioning damage state ( $DS_{MS}$ ) while the line color represents the achieved damage state ( $DS_{AS}$ ). For example, the red dotted line represents  $DS_{MS} = 1$  and  $DS_{AS} = 4$

Figure 8b shows the hysteretic energy versus maximum interstorey drift scatter for the four-storey infilled frames (beam-, mixed- and column-sway). The hysteretic energy is normalized with respect to the product of the base shear and displacement at DS4 (called  $F_u \Delta_u$ ). This is done because  $F_u \Delta_u$  is explicitly dependent on the plastic mechanism of the structure (and somehow proportional to number of involved members; e.g. smaller for a soft storey with respect to a global mechanism). Moreover, this parameter can give a proxy for the number of plastic cycles. Two alternative normalizations are added to allow comparisons with previous studies: (a) with respect to the product of the base shear and displacement at yielding ( $DS2, F_y \Delta_y$ ); (b) with respect to the total mass  $M$ , which gives the equivalent velocity  $v = \sqrt{2E_{H,MS}/M}$ , consistent with energy-based design.<sup>8</sup>

Confirming the discussion in Section 2, the degrading behavior of the case studies has a pronounced effect on the hysteretic energy versus maximum interstorey drift relationship. Indeed, such relationship (regardless of the adopted normalization) has an asymptotic behavior for the shown column-sway case, unlike the beam- and mixed-sway frames, which show a considerably lower degradation (within the range of the analyzed drift values). Such an asymptotic behavior is also theoretically expected for beam- and mixed-sway frames, although this would emerge for unphysically large values of the drift.

According to Section 3, a PSDM and a set of state-dependent fragility curves are derived for each case study. To drive the discussion, Figure 9 shows the fragility curves for the four-storey beam-, mixed-, and column-sway bare frames, together with the mixed-sway, infilled one. Moreover, the parameters of both the PSDM and the fragility curves for all the case studies are listed in Table 2 for all the case studies. It is worth mentioning that the DS3 and DS4 fragility curves for the four-storey, infilled beam-sway frame are deemed less reliable as the PSDM is used to extrapolate with respect to the analysis data. Both the PSDMs and the fragility curves are derived adopting  $avgSA$  as an IM. In particular,  $avgSA$  is

TABLE 2 Parameters of the probabilistic seismic demand models and the state dependent fragilities

	Four storeys							Eight storeys						
	Bare			Uniformly infilled			Pilotis	Bare			Uniformly infilled			Pilotis
	BS	MS	CS	BS	MS	CS		BS	MS	CS	BS	MS	CS	
$a$	0.79	2.27	2.09	1.15	2.32	2.20	1.75	0.36	0.61	3.20	0.59	0.84	2.49	2.33
$b$	1.38	1.37	1.32	1.20	1.17	1.26	1.23	1.64	1.78	1.54	1.29	1.27	1.22	1.27
$c_0$	1.92	6.66	32.65	0.89	1.89	2.74	19.89	4.66	1.97	57.16	2.71	2.36	6.27	20.21
$d$	1.68	1.68	1.60	1.24	1.03	1.91	1.47	1.85	2.07	1.92	1.67	1.65	1.83	1.65
$m$	0.20	0.15	0.26	0.19	0.16	0.78	0.21	0.15	0.35	0.88	0.18	0.19	0.65	0.43
$\beta$	0.36	0.35	0.36	0.38	0.46	0.26	0.37	0.24	0.24	0.28	0.30	0.30	0.24	0.35
$\mu(\text{DS1})$	0.03	0.03	0.02	0.05	0.02	0.13	0.02	0.04	0.12	0.02	0.02	0.02	0.07	0.03
$\mu(\text{DS2})$	0.18	0.14	0.09	0.25	0.18	0.29	0.10	0.10	0.22	0.08	0.10	0.13	0.19	0.11
$\mu(\text{DS2} \text{DS1})$	0.18	0.13	0.08	0.22	0.16	0.26	0.09	0.09	0.19	0.08	0.10	0.13	0.17	0.10
$\mu(\text{DS3})$	1.09	0.33	0.14	3.12	0.77	0.64	0.15	0.66	0.38	0.16	0.98	0.39	0.47	0.21
$\mu(\text{DS3} \text{DS1})$	1.09	0.33	0.13	3.13	0.75	0.63	0.15	0.66	0.38	0.16	0.98	0.39	0.46	0.21
$\mu(\text{DS3} \text{DS2})$	1.09	0.29	0.10	3.10	0.62	0.60	0.10	0.66	0.34	0.15	0.98	0.36	0.44	0.18
$\mu(\text{DS4})$	1.42	0.42	0.17	3.84	1.07	0.79	0.20	0.86	0.49	0.21	1.25	0.49	0.63	0.27
$\mu(\text{DS4} \text{DS1})$	1.42	0.42	0.17	3.84	1.05	0.79	0.19	0.86	0.50	0.21	1.26	0.49	0.63	0.27
$\mu(\text{DS4} \text{DS2})$	1.43	0.39	0.15	3.84	0.93	0.79	0.16	0.87	0.48	0.22	1.27	0.47	0.63	0.25
$\mu(\text{DS4} \text{DS3})$	1.06	0.23	0.10	2.04	0.35	0.62	0.10	0.70	0.37	0.21	1.07	0.26	0.53	0.17

Abbreviations: BS, beam sway; MS, mixed sway; CS, column sway. Shaded cells refer to extrapolation with respect to the range of the analysis data

calculated in the range  $[0.2T_1 - 1.5T_1]$  for the bare frames (including the column-sway, pilotis ones) and  $[0.2T_1 - 3.0T_1]$  for the infilled frames.

For all the case studies, as expected, a particularly low level of damage (DS1) does not cause a shift of the AS fragilities for all the other DSs. However, higher levels of damage (DS2 or DS3) have particularly different effects depending on the considered case study. As expected, the beam-sway frames (i.e. code-compliant, newly-designed structures) are only slightly affected by damage accumulation, likely due to their particularly stable hysteresis governed by the flexure in the beams. As shown in Figure 9a a higher DS in the MS essentially caused no shift in the AS fragility medians. The only exception is the DS4 median given DS3 in the MS. Although this corresponds to a 25% reduction of the DS4 fragility median for the MS, this is unlikely to be relevant for practical purposes because the DS4|DS3 median is still sufficiently high. Moreover, if such a structure experiences a DS3 due to the MS, it is likely to be tagged as unsafe to occupy in the aftermath of the MS.

On the other hand, column-sway frames (Figure 9c) are considerably affected by damage accumulation, given their unstable hysteretic behavior and the pronounced strength degradation. The DS3 fragility median in the MS is reduced by 30% if DS2 is registered in the MS (DS3|DS2 fragility). The reduction is equal to 47% for the DS4|DS3 fragility. In absolute terms, however, this effect corresponds to a small reduction in the median capacity, as the MS fragilities of this type of uncompliant buildings (exhibiting a soft-storey behavior) are particularly low. Therefore, damage accumulation may be practically less relevant in this case, as this type of structures is likely to sustain a large DS in the MS, and likely to be tagged as unsafe.

The mixed-sway frames (Figure 9b), showing unstable hysteretic behavior likely governed by shear failures in the joint panels, display a peculiar behavior related to damage accumulation effects. For such an underdesigned case study, which does not develop a soft-storey mechanism, the DS4|DS3 fragility median is 47% smaller than the DS4 median in the MS (12% reduction from DS2 to DS3|DS2). Given the higher median capacity with respect to the column-sway frames, damage accumulation is likely to be particularly relevant, in absolute terms, for this case study. This effect is amplified by the presence of the infills (Figure 9d), which strongly govern the hysteretic behavior of the frame for small displacements. In fact, a level of damage equal to DS3 corresponds to the (almost complete) degradation of the infills. As an approximation, if such a case study experiences a DS3 in the MS, it will behave as a bare frame in the AS. Indeed, the DS4|DS3 median capacity of the mixed-sway, infilled frame is approximately equal to the DS4 median capacity of the corresponding bare frame in the MS. In relative terms, the median capacity of the DS4|DS3 fragility is reduced by 70% with respect to the DS4 median capacity in the MS. The effect of the infills is qualitatively similar for the beam-sway and mixed-sway case studies.

The column-sway pilotis frames are not discussed in detail as they effectively behave like the column-sway, bare frames (already discussed).

It is noted that each eight-storey case study is considerably less affected by damage accumulation, if compared with the corresponding four-storey frame with the same properties. This is likely due to a loss of efficiency of  $avgSA$  in the AS, with respect to the MS. In particular, the MS is likely to cause a period elongation of the structure, mainly affecting the vibration mode compatible with the developed plastic mechanism. In the AS, the relative influence of higher vibration modes changes with respect to the MS. As the period range for  $avgSA$  is based on undamaged conditions, period elongation causes the above-mentioned loss of efficiency of the IM.

## 5 | CONCLUSIONS

This paper has introduced a novel framework for the derivation of state-dependent fragility relationships for structures subjected to MS-AS ground motion sequences. The total hysteretic energy dissipated in the ground-motion sequence is adopted as the main demand parameter in the proposed framework. This is because hysteretic energy is a cumulative measure that monotonically increases with the length of the applied excitation. Unlike peak parameters (e.g. maximum interstorey drift), this allows one to develop statistical models consistent with the physics of a structure subjected to ground motion sequences.

Based on the analysis of simple case studies, the hysteretic energy versus peak deformation relationship has been discussed, highlighting two important features: (a) the significant duration of the ground motion may be adopted to explain the variability of the hysteretic energy for a given peak deformation; (b) in the AS, a structure dissipates less energy (for a given peak displacement in the AS) if the peak displacement in the MS is higher.

Based on the first consideration, it was proposed to use the median hysteretic energy vs. peak deformation relationship for a given structure to convert the deformation-based DS thresholds into energy-based ones. This allows calculating fragility relationships in energy terms while retaining the confidence of widely accepted/calibrated deformation-based DS thresholds.

A PSDM was proposed in the form of a surface relating the hysteretic energy dissipated in the sequence to the peak deformation (e.g. maximum interstorey drift) in the MS and an IM of the AS (which may be a spectral acceleration or the geometric mean of the spectral acceleration in a range of periods). Such function is consistent with the relevant mechanics as the median hysteretic energy dissipated during the sequence is monotonic with respect to (any combination of) the maximum response in the MS and the IM of the AS; and the hysteretic energy dissipated in the AS is lower if the peak deformation in the MS is higher. The proposed model may be considered as a generalization of the power-law relationship commonly adopted for cloud-based MS-only problems (it provides the same answer if it is used to predict MS fragility curves).

The proposed framework was demonstrated for 14 RC frame buildings, characterized by different height levels (four or eight storeys), plastic mechanisms (beam sway, in which all the beams are yielding; column sway, with a soft-storey mechanism; mixed sway, in which a combination of beam, column, and/or joint failures can be triggered), configuration of the infill panels (bare frame, uniformly infilled frame, pilotis frame). Overall, the results confirmed the feasibility of the proposed approach, which allows considering damage accumulation without inconsistencies in the statistical model. It is shown that, for a given structure, a sufficiently large number of ground-motion records, with appropriate distributions of the geometric mean of the spectral acceleration and the significant duration, enables to fully characterize the structural response in energy terms, allowing one to capture the accumulation of damage. The results for the considered case-study structures highlighted that, for a given representative geometry, the plastic mechanism is the most influencing parameter to consider in the energy-based seismic response characterization, followed by the height of the building. The infill distribution has also a nonnegligible influence. However, a pilotis frame is likely to behave as a column-sway bare frame.

The proposed framework may be used for risk models that explicitly consider MS-AS sequences, both related to single structures or large portfolios. Frameworks similar to the proposed one may be derived for problems involving long-duration ground motions or very soft soils, exploiting the features of the hysteretic energy versus peak deformation relationship.

## ACKNOWLEDGMENTS

This study was performed within the framework of the European Union's Horizon 2020 research and innovation programme under grant agreement No. 843794. (Marie Skłodowska-Curie Research Grants Scheme MSCA-IF-2018:

MULTIRES, MULTI-level framework to enhance seismic RESilience of RC buildings) for RG; and within the framework of the project “Dipartimenti di Eccellenza”, funded by the Italian Ministry of Education, University and Research at IUSS Pavia, for CG.

## ORCID

Roberto Gentile  <https://orcid.org/0000-0002-7682-4490>

Carmine Galasso  <https://orcid.org/0000-0001-5445-4911>

## REFERENCES

- Cosenza E, Manfredi G. Damage indices and damage measures. *Prog Struct Mater Eng*. 2000;2(1):50-59. [https://doi.org/10.1002/\(sici\)1528-2716\(200001/03\)2:1<50::aid-pse7>3.3.co;2-j](https://doi.org/10.1002/(sici)1528-2716(200001/03)2:1<50::aid-pse7>3.3.co;2-j).
- Fajfar P. Equivalent ductility factors, taking into account low-cycle fatigue. *Earthq Eng Struct Dyn*. 1992;21(10):837-848. <https://doi.org/10.1002/eqe.4290211001>.
- Papadopoulos AN, Kohrangi M, Bazzurro P. Mainshock-consistent ground motion record selection for aftershock sequences. *Earthq Eng Struct Dyn*. 2019;49:754-771. <https://doi.org/10.1002/eqe.3263>.
- Di Trapani F, Malavisi M. Seismic fragility assessment of infilled frames subject to mainshock/aftershock sequences using a double incremental dynamic analysis approach. *Bull Earthq Eng*. 2019;17(1):211-235. <https://doi.org/10.1007/s10518-018-0445-2>.
- Aljawhari K., Gentile R., Freddi F., Galasso C., Effects of Ground-motion Sequences on the Vulnerability of Case-Study Reinforced Concrete Frames, *Bulletin of Earthquake Engineering*, <https://doi.org/10.1007/s10518-020-01006-8> (in press).
- Zhang L, Goda K, De Luca F, De Risi R. Mainshock-aftershock state-dependent fragility curves: a case of wood-frame houses in British Columbia, Canada. *Earthq Eng Struct Dyn*. 2020;49(9):884-903. <https://doi.org/10.1002/eqe.3269>.
- Changhai Z, Duofa J, Weiping W, Cuihua L, Weidong L, Lili X. Hysteretic energy prediction method for mainshock-aftershock sequences. *Earthq Eng Eng Vib*. 2018;17(2):277-291.
- Housner GW, Limit design of structures to resist earthquakes. Paper presented at: First World Conference on Earthquake Engineering, San Francisco, California, 1956.
- Chai YH. Incorporating low-cycle fatigue model into duration-dependent inelastic design spectra. *Earthq Eng Struct Dyn*. 2005;34(1):83-96. <https://doi.org/10.1002/eqe.422>.
- Malhotra PK. Cyclic-demand spectrum. *Earthq Eng Struct Dyn*. 2002;31(7):1441-1457. <https://doi.org/10.1002/eqe.171>.
- Kunnath SK, Chai YH. Cumulative damage-based inelastic cyclic demand spectrum. *Earthq Eng Struct Dyn*. 2004;33(4):499-520. <https://doi.org/10.1002/eqe.363>.
- Uang C-M, Bertero VV. Evaluation of seismic energy in structures. *Earthq Eng Struct Dyn*. 1990;19(1):77-90. <https://doi.org/10.1002/eqe.4290190108>.
- Decanini LD, Mollaioli F, Saragoni R, Energy and displacement demands imposed by near-source ground motions. Paper presented at: 12th World Conference on Earthquake Engineering, vol. 30, Auckland, New Zealand: 2000.
- Quinde P, Terán-Gilmore A, Reinoso E. Cumulative structural damage due to low cycle fatigue: an energy-based approximation. *J Earthq Eng*. 2019;1-21. <https://doi.org/10.1080/13632469.2019.1692736>.
- Terán Gilmore A. Consideraciones De Uso De La Energía Plástica En El Diseño Sísmico (in Spanish). *Revista de Ingeniería Sísmica*. 2001;110(65):81.
- Erberik A, Sucuoğlu H. Seismic energy dissipation in deteriorating systems through low-cycle fatigue. *Earthq Eng Struct Dyn*. 2004;33(1):49-67. <https://doi.org/10.1002/eqe.337>.
- Gosain NK, Brown RH, Jirsa JO. Shear requirements for load reversals on RC members. *J Struct Div ASCE*. 1977; 103: 1461-1476.
- Scribner CF, Wight JK. Strength decay in R. C. beams under load reversals. *J Struct Div ASCE*. 1980; 106: 861-875.
- Darwin D, Nmai CK. Energy dissipation in R.C. beams under cyclic loadings. *Eng Fract Mech*. 1986;39(8):177-184. [https://doi.org/10.1016/0013-7944\(91\)90033-W](https://doi.org/10.1016/0013-7944(91)90033-W).
- Akiyama H. *Earthquake-Resistant Limit-State Design for Buildings*. Tokyo, Japan: University of Tokyo Press (Japanese version 1980; English version 1985); 1980.
- Priestley M. Myths and fallacies in earthquake engineering - conflicts between design and reality. *Bull NZ Soc Earthq Eng*. 1993;26(3):329-341.
- Kazantzi AK, Vamvatsikos D. The hysteretic energy as a performance measure in analytical studies. *Earthq Spectra*. 2018;34(2):719-739. <https://doi.org/10.1193/112816EQS207M>.
- Vamvatsikos D, Allin Cornell C. Incremental dynamic analysis. *Earthq Eng Struct Dyn*. 2002;31:491-514. <https://doi.org/10.1002/eqe.141>.
- Saiidi M, Sozen M, *Simple and Complex Models for Nonlinear Seismic Response of Reinforced Concrete Structures*. Urbana, IL: University of Illinois at Urbana-Champaign; 1979.
- Nakashima M, Saburi K, Tsuji B. Energy input and dissipation behaviour of structures with hysteretic dampers. *Earthq Eng Struct Dyn*. 1996;25(November 1995):483-496.
- Smerzini C, Galasso C, Iervolino I, Paolucci R. Ground motion record selection based on broadband spectral compatibility. *Earthq Spectra*. 2014;30(4):1427-1448. <https://doi.org/10.1193/052312EQS197M>.

27. Gentile R, Galasso C, Idris Y, Rusydy I, Meilianda E. From rapid visual survey to multi-hazard risk prioritisation and numerical fragility of school buildings. *Natl Hazards Earth Syst Sci*. 2019;19:1365-1386. <https://doi.org/10.5194/nhess-2018-397>.
28. Riddell R, Garcia JE. Hysteretic energy spectrum and damage control. *Earthq Eng Struct Dyn*. 2001;30(12):1791-1816. <https://doi.org/10.1002/eqe.93>.
29. Bojórquez E, Terán-Gilmore A, Ruiz SE, Reyes-Salazara A. Evaluation of structural reliability of steel frames: interstorey drift versus plastic hysteretic energy. *Earthq Spectra*. 2011;27(3):661-682. <https://doi.org/10.1193/1.3609856>.
30. Jalayer F, Ebrahimian H, Miano A, Manfredi G, Sezen H. Analytical fragility assessment using unscaled ground motion records. *Earthq Eng Struct Dyn*. 2017;46(15):2639-2663. <https://doi.org/10.1002/eqe.2922>.
31. Tsioulou A, Taflanidis AA, Galasso C. Hazard-compatible modification of stochastic ground motion models. *Earthq Eng Struct Dyn*. 2018;47:1774-1798. <https://doi.org/10.1002/eqe.3044>.
32. Goda K. Record selection for aftershock incremental dynamic analysis. *Earthq Eng Struct Dyn*. 2015;44:1157-1162. <https://doi.org/10.1002/eqe.2513>.
33. Goda K, Taylor CA. Effects of aftershocks on peak ductility demand due to strong ground motion records from shallow crustal earthquakes. *Earthq Eng Struct Dyn*. 2012. <https://doi.org/10.1002/eqe.2188>.
34. Minas S, Galasso C. Accounting for spectral shape in simplified fragility analysis of case-study reinforced concrete frames. *Soil Dyn Earthq Eng*. 2019;119:91-103. <https://doi.org/10.1016/j.soildyn.2018.12.025>.
35. Priestley MJN, Calvi GM, Kowalsky MJ. *Displacement-based Seismic Design of Structures*. Pavia, Italy: IUSS Press; 2007.
36. NZS 1170.5:2004, Structural design actions, Part 5 - Earthquake actions. <https://www.standards.govt.nz/sponsored-standards/building-standards/NZS1170-5>. Standards New Zealand, Wellington, New Zealand. 2004.
37. NZS 3101. Part 1: Concrete structures standard - The design of concrete structures. <https://www.standards.govt.nz/sponsored-standards/building-standards/NZS3101-1-and-2>. Standards New Zealand, Wellington, New Zealand 2006.
38. Gentile R, Pampanin S, Raffaele D, Uva G. Non-linear analysis of RC masonry-infilled frames using the SLaMA method: part 2—parametric analysis and validation of the procedure. *Bull Earthq Eng*. 2019;17(6):3305-3326. <https://doi.org/10.1007/s10518-019-00584-6>.
39. Kircher CA, Whitman RV, Holmes WT. HAZUS earthquake loss estimation methods. *Nat Hazards Rev*. 2006;7(2):45-59. [https://doi.org/10.1061/\(asce\)1527-6988\(2006\)7:2\(45\)](https://doi.org/10.1061/(asce)1527-6988(2006)7:2(45)).
40. Carr AJ, RUAUMOKO2D - The Maori God of Volcanoes and Earthquakes. Inelastic Analysis Finite Element program. Christchurch, New Zealand; 2016.
41. Calvi GM, Magenes G, Pampanin S, Experimental test on a three storey RC frame designed for gravity only. Paper presented at: 12th European Conference on Earthquake Engineering, vol. 727, 2002; London, UK.
42. Sharpe RD. *The Seismic Response of Inelastic Structures*. PhD dissertation. Christchurch, New Zealand: Department of Civil Engineering, University of Canterbury; 1976.
43. Gentile R, RC section rect—practical manual. Free internal report and software. 2017; <http://www.robortogentile.org>. Accessed July 30, 2019.
44. Gentile R, Del Vecchio C, Pampanin S, Raffaele D, Uva G. Refinement and validation of the simple lateral mechanism analysis (SLaMA) procedure for RC frames. *J Earthq Eng*. 2019;1-29.
45. Crisafulli FJ. *Seismic Behaviour of Reinforced Concrete Structures with Masonry Infills*. PhD dissertation, New Zealand: University of Canterbury; 1997.
46. Gentile R, Pampanin S, Raffaele D, Uva G. Non-linear analysis of RC masonry-infilled frames using the SLaMA method: part 1—mechanical interpretation of the infill/frame interaction and formulation of the procedure. *Bull Earthq Eng*. 2019;17(6):3283-3304. <https://doi.org/10.1007/s10518-019-00580-w>.
47. Gentile R, Pampanin S, Raffaele D, Uva G. Analytical seismic assessment of RC dual wall/frame systems using SLaMA: proposal and validation. *Eng Struct*. 2019;188:493-505. <https://doi.org/10.1016/j.engstruct.2019.03.029>.

**How to cite this article:** Gentile R, Galasso C. Hysteretic energy-based state-dependent fragility for ground-motion sequences. *Earthquake Engng Struct Dyn*. 2020;1–17. <https://doi.org/10.1002/eqe.3387>